ISSN 1846-6168 (Print), ISSN 1848-5588 (Online)
https://doi.org/10.31803/tg-20250226133036

Original scientific paper
Received: 2025-02-26, Accepted: 2025-04-29

Ball and Plate Mechanism Actuated with Pneumatic Artificial Muscles

Juraj Benić*, Andreas Šantek, Željko Šitum

Abstract: A novel ball-and-plate mechanism actuated with pneumatic artificial muscles is presented in this paper. The pneumatic muscles are arranged in two antagonistic configuration pairs to generate torque around two axes of plate rotation. The ball-and-plate system is classified as an under-actuated, high-order nonlinear system, with additional nonlinearities introduced by the air compressibility of the pneumatic muscles. A nonlinear mathematical model of the ball-and-plate system has been derived, in which the proposed system is modelled as two ball-and-beam systems, each representing one direction of the ball's movement. Along with the nonlinear equations of motion, a simplified dynamical model of the pneumatic muscles and the proportional valve is included. The linearized model is developed and represented in a state-space form, which is used for LQR controller synthesis. The proposed controller is tested through numerical simulations and experimentally validated on the developed ball-and-plate mechanism setup.

Keywords: ball and plate; LQR; mathematical modeling; pneumatics muscles

1 INTRODUCTION

The ball-and-plate system is an extension of the two-degrees-of-freedom (DOF) ball-and-beam system [1] to a four-DOF problem. This system is considered a benchmark problem in control theory due to its nonlinear, multivariable, under-actuated, and unstable open-loop dynamics. The control challenges associated with the ball-and-plate system are typically divided into two categories: point stabilization [2] and trajectory tracking [3]. Various control methods have been applied to address these challenges, including PID controllers [4], LQR regulators [5], sliding mode controllers [6], model reference adaptive controllers [7], fuzzy controllers [8], neural networks and genetic algorithms [9], and, more recently, linear matrix inequalities [10].

From a pneumatic perspective, the ball-and-beam system with two pneumatic cylinders as actuators and a fuzzy P(I)D regulator was investigated in [11]. Similarly, in [12], the pneumatic cylinders were replaced with pneumatic artificial muscles (PAMs), and an LQR regulator was used to stabilize the system. In [13], researchers extended this approach by using two pneumatic cylinders to actuate a ball-and-plate mechanism. However, a review of the literature indicates that PAMs have not been used to stabilize a ball-and-plate mechanism.

PAMs are highly nonlinear pneumatic actuators due to their construction and the compressibility of air within them [14]. Their lightweight construction, high power-to-weight ratio, and ability to operate in explosive or hazardous environments make them ideal for medical and industrial applications. Over the years, many types of PAMs have been developed, including McKibben, Yarlott, Kukolj, Festo PAMs, and others. In this paper, Festo PAMs are used to actuate the ball-and-plate system, introducing additional nonlinearity to an already complex system.

This study addresses both the stabilization and trajectory tracking problems of a ball-and-plate mechanism actuated by four PAMs. It builds on our previous work described in [12]. Two antagonistic groups of pneumatic muscles are used to generate torque and achieve rotation about the plate's horizontal axis. An LQR regulator is employed to stabilize this highly nonlinear system. The regulator's performance is evaluated through two test scenarios: stabilizing the ball at the plate's center and having the ball follow a circular trajectory.

The remainder of this paper is organized as follows: Section 2 provides a detailed description of the experimental setup, while Section 3 outlines the mathematical modeling procedure for the proposed system. Section 4 presents experimental and simulation results, while conclusions and directions for future work are discussed in Section 5.

2 EXPERIMENTAL SETUP

The proposed ball-and-plate system, shown in Fig. 1, was developed in the Automation and Robotics Laboratory at the Faculty of Mechanical Engineering and Naval Architecture. The experimental setup serves both as a platform for research in pneumatic systems control and as a training tool for students.

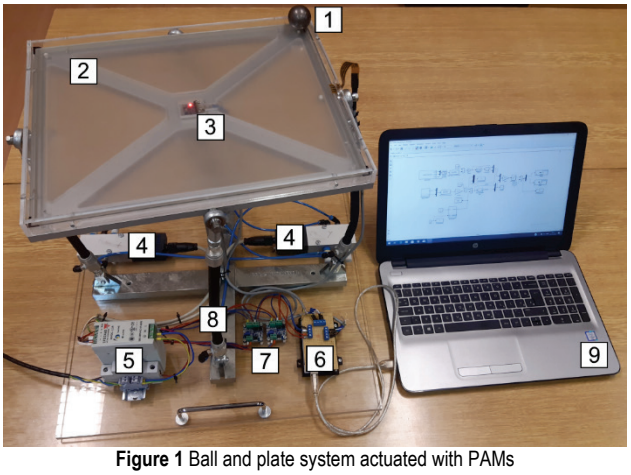

Figure 1 Ball and plate system actuated with PAMs

The experimental setup, shown in Fig. 1, consists of a steel ball (1) placed on a resistive four-wire analog 17-inch touchscreen (2). The position of the ball is detected by measuring the voltage drop (ranging from 0 to 5 V) across the X and Y axes. These measurements are processed by an Arduino Mega 2560 microcontroller (6). A key limitation of

the resistive touchscreen is its inability to simultaneously measure both coordinates. This issue is resolved by measuring each position separately with a 1-microsecond delay, allowing sufficient time for voltage stabilization across the second axis. The touchscreen is mounted on a transparent plexiglass sheet, which is secured to a CNC-milled aluminum frame.

Angular velocity is measured using the widely utilized MPU 6050 gyroscope (3), which is also integrated into the aluminum frame. The MPU 6050 combines a three-axis gyroscope and a three-axis accelerometer in a single unit, offering four programmable angular velocity ranges (measured in degrees per second) and a built-in digital programmable low-pass filter. The gyroscope communicates with the microcontroller via the I2C protocol.

Two pairs of pneumatic artificial muscles (PAMs) (8) (Festo, type DMSP-10-200N-RM-CM) are arranged antagonistically to actuate a spherical joint. The torque required for plate actuation is achieved by creating a pressure differential between the pairs of PAMs, which causes the plate to rotate around the X and Y axes. This pressure differential is regulated by two proportional 5/3 control valves (4) (Festo, type MPYE-5 1/8 HF-010B), connected to a 24 VDC power supply (5).

To control the spool movement in the valves, an analog control signal ranging from 0 to 10 V is required. The flow rate and thus the pressure differential in the PAMs is adjusted by the spool's movement. The Arduino microcontroller generates a PWM signal in the range of 0 to 5 VDC. This PWM signal is converted to an analog signal (0 to 10 VDC) using two PWM-to-voltage converters (7), each controlling one proportional valve. By default, the Arduino's PWM output is set to 2.5 VDC, which, after conversion, provides 5 VDC to the valves, positioning the spools in their neutral state and maintaining approximately equal pressures in the muscles.

The controller is implemented using the MATLAB Simulink software installed on a PC (9). The control process utilizes custom-built blocks for the touchscreen, an additional library for the MPU 6050 gyroscope, and the Simulink Support Package for Arduino.

3 MATHEMATICAL MODELING

To achieve successful control of the ball-and-plate system, it is essential to derive a nonlinear mathematical model of the system. The following assumptions are made to simplify the analysis:

- the ball is an ideal sphere with a constant radius,
- the ball remains in continuous contact with the plate,
- there is no slipping between the ball and the plate,
- friction is negligible,
- the height of the plate is negligible.

The nonlinear dynamic model of the system is derived using the Lagrange method, where the Lagrange equation is expressed as:

$$L = K - P, \tag{1}$$

where K and P represent the total kinetic and potential energy of the system, respectively. The derivative of the Lagrangian is given by:

$$\frac{\mathrm{d}}{\mathrm{d}t}\left(\frac{\partial L}{\partial \dot{q}_i}\right) - \frac{\partial L}{\partial q_i} = T_i, \tag{2}$$

where q_i represents the generalized coordinates, and T_i is the moment around the corresponding generalized coordinate. Four generalized coordinates are defined as follows: $q_1 = x$ and $q_2 = y$ (representing the ball's position on the plate), and $q_3 = \theta_1$ and $q_4 = \theta_2$ (representing the plate angles around the X and Y axes). A schematic representation of the proposed system and the generalized coordinates is provided in Fig. 2.

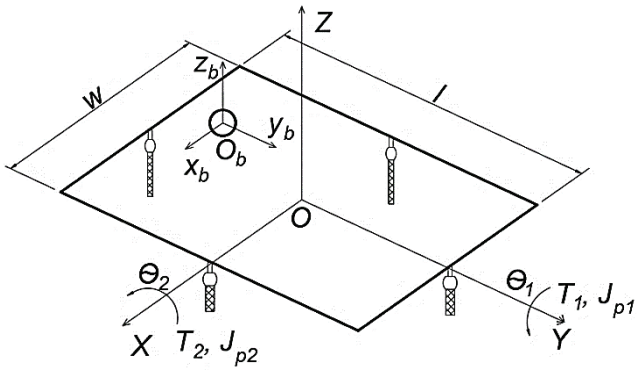

Figure 2 Schematic representation of ball on plate setup

The mathematical model of the experimental setup can be further simplified by representing the ball-and-plate system as two ball-and-beam systems. The first system moves the ball in the Y-direction, while the second moves it in the X-direction. The proposed simplified model of the ball-and-plate system is shown in Fig. 3, where the ball moves in the local OX_iY_i frame, with i indicating the number of the ball-and-beam system.

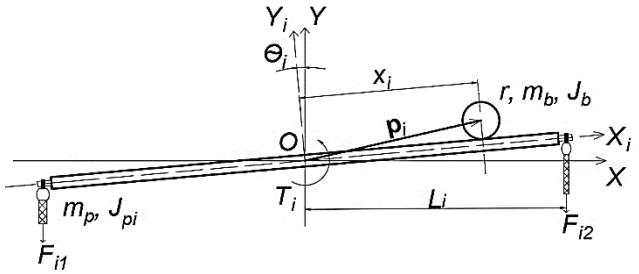

Figure 3 The ball on plate representation with a two ball on beam systems

The kinetic and potential energy of the proposed simplified model of the beam can be expressed as follows:

$$\begin{aligned} K_{pi} &= \frac{1}{2} J_{pi} \dot{\theta}_i^2, \\ P_{pi} &= 0, \end{aligned} \tag{3}$$

where K_{pi} and P_{pi} represent the kinetic and potential energy of the plate, modeled as two beams. $\dot{\theta}_i$ is the angular velocity

of the plate, and J_{pi} is the moment of inertia of the beam around the center of rotation, defined as:

$$J_{pi} = m_p \frac{l_i^2}{12}, \tag{4}$$

where m_p is plate mass and l_i is the length or width of the plate, depending on the X or Y axis as shown in Fig. 2. From Eq. (3) and Eq. (4), the total kinetic and potential energy of the plate can be defined as:

$$\begin{aligned} K_p &= \frac{1}{24} m_p \left(l^2 \dot{\theta}_2^2 + w^2 \dot{\theta}_1^2 \right), \\ P_p &= 0, \end{aligned} \tag{5}$$

where l and w are the length and width of the plate, respectively. The potential energy of the plate is considered zero due to the placement of the $OXYZ$ coordinate system at the center of gravity of the plate.

The potential energy of the ball, as shown in Fig. 3, can be expressed as follows:

$$P_{bi} = m_b \mathrm{g} \left(x_i \sin(\theta_i) + r \cos(\theta_i) \right), \tag{6}$$

where m_b and r are the mass and radius of the ball, respectively, g s the gravitational constant, θ_i is the plate angle, and x_i is the position of the plate in OX_iY_i frames. From Eq. (7), the total potential energy of the ball is derived as:

$$P_b = m_b \mathrm{g} \left[x \sin(\theta_1) + y \sin(\theta_2) + r \left(\cos(\theta_1) + \cos(\theta_2) \right) \right], \tag{7}$$

where x and y are the positions of the ball on the plate.

The kinetic energy of the ball consists of both translational and rotational energy and is expressed as:

$$K_{bi} = \frac{1}{2} m_b v_i^2 + \frac{1}{2} J_b \omega_i^2, \tag{8}$$

where $J_b = 2m_b r^2/5$ is the moment of inertia of a solid sphere, v_i is the translational velocity of the ball, and ω_i is the peripheral speed of the ball, defined as:

$$\omega_i = \frac{\dot{x}_i}{r}. \tag{9}$$

From Eq. (8) and Eq. (9), the kinetic energy of the ball is expressed as:

$$K_{bi} = \frac{1}{2} m_b v_i^2 + \frac{1}{2} \frac{J_b}{r^2} \dot{x}_i^2. \tag{10}$$

The translational velocity of the ball is derived from the position vector $\boldsymbol{p}_i$ which connects the origin of the OXY frame to the center of the ball. From Fig. 3, using the rotation matrix around the Z-axis, the vector $\boldsymbol{p}_i$ can be written as:

$$\boldsymbol{p}_i = \begin{bmatrix} x_i \cos(\theta_i) - r \sin(\theta_i) \\ x_i \sin(\theta_i) + r \cos(\theta_i) \end{bmatrix}, \tag{11}$$

and its derivative can be written as:

$$\dot{\boldsymbol{p}}_i = v_i = \begin{bmatrix} \dot{x}_i \cos(\theta_i) - x_i \dot{\theta}_i \sin(\theta_i) - r \dot{\theta}_i \cos(\theta_i) \\ \dot{x}_i \sin(\theta_i) + x_i \dot{\theta}_i \cos(\theta_i) - r \dot{\theta}_i \sin(\theta_i) \end{bmatrix}. \tag{12}$$

From Eq. (12) v_i^2 is obtained as:

$$v_i^2 = \dot{x}_i^2 - 2r\dot{x}_i\dot{\theta}_i + r^2\dot{\theta}_i^2 + x^2\dot{\theta}^2. \tag{13}$$

Inserting Eq. (13) into Eq. (10) yields:

$$K_{bi} = \frac{1}{2} m_b \left(\dot{x}_i^2 - 2r\dot{x}_i\dot{\theta}_i + r^2\dot{\theta}_i^2 + x^2\dot{\theta}^2 \right) + \frac{1}{2} \frac{J_b}{r^2} \dot{x}_i^2. \tag{14}$$

From Eq. (14) kinetic energy of the ball in the global coordinate system from Fig. 2, is expressed as:

$$\begin{aligned} K_b = {} & \frac{1}{2} \left(m_b + \frac{J_b}{r^2} \right) (\dot{x}^2 + \dot{y}^2) + \\ & + \frac{1}{2} m_b \left(x^2\dot{\theta}_1^2 - 2rx\dot{\theta}_1 + r^2\dot{\theta}_1^2 + y^2\dot{\theta}_2^2 - 2ry\dot{\theta}_2 + r^2\dot{\theta}_2^2 \right). \end{aligned} \tag{15}$$

From Eq. (5), Eq. (7), and Eq. (15), the total kinetic and potential energy is defined as:

$$\begin{aligned} K &= K_p + K_b, \\ P &= P_p + P_b. \end{aligned} \tag{16}$$

From Eq. (2) to Eq. (16), and with the previously defined generalized coordinates, the nonlinear mathematical model of the ball-and-plate system is obtained as follows:

$$\begin{aligned} & \left(m_b + \frac{J_b}{r^2} \right) \ddot{q}_1 - m_b r \ddot{q}_3 - m_b q_1 \dot{q}_3^2 + \mathrm{g} m_b \sin(q_3) = 0, \\ & \left(m_b + \frac{J_b}{r^2} \right) \ddot{q}_2 - m_b r \ddot{q}_4 - m_b q_2 \dot{q}_4^2 + \mathrm{g} m_b \sin(q_4) = 0, \\ & \left(m_p \frac{w^2}{12} + m_b r^2 + m_b q_1^2 \right) \ddot{q}_3 + m_b (2q_1\dot{q}_1\dot{q}_3 - r\ddot{q}_1) + \\ & + m_b \mathrm{g} \left(q_1 \cos(q_3) - r \sin(q_3) \right) = T_1, \\ & \left(m_p \frac{w^2}{12} + m_b r^2 + m_b q_2^2 \right) \ddot{q}_4 + m_b (2q_2\dot{q}_2\dot{q}_4 - r\ddot{q}_2) + \\ & + m_b \mathrm{g} \left(q_2 \cos(q_4) - r \sin(q_4) \right) = T_2. \end{aligned} \tag{17}$$

The applied torque T_i (Fig. 3) for rotating the beam can be calculated from the muscle contraction forces F_{i1} and F_{i2} as derived in [12, 15, 16], using the following expression:

$$T_i = K_i \Delta p_i, \tag{18}$$

where Δp_i is the pressure difference inside the PAMs, and K_i is defined as:

$$K_i = \frac{\pi}{2} L_i D_0^2 \left[3\tan^2(\alpha_0)\left(1-\epsilon_0\right)^2 - \sin^2(\alpha_0) \right], \tag{19}$$

where L_i is the distance from the center of rotation, D_0 and ϵ_0 are the nominal diameter and initial contraction ratio of the PAMs, respectively, and α_0 is the initial angle of the braided shell between the thread and the long axis of the PAM.

The pressure dynamics in the PAMs can be represented by the first-order lag term as:

$$\tau_v \Delta \dot{p}_i + \Delta p_i = K_v u_i, \tag{20}$$

where K_v and τ_v are the valve gain and time constant, respectively, and u_i is the input voltage to the pneumatic proportional valve.

3.1 Linearized Mathematical Model

The linearized equations of motion around the equilibrium state will be derived from Eq. (17). The assumptions on which the linear model is based are:

- small angles of rotation: $\sin(\Delta q_i) \cong \Delta q_i$ and $\cos(\Delta q_i) \cong 1$
- small angular velocity: $\dot{q}_3 \cong \dot{q}_4 \cong 0$
- small ball displacements: $q_1^2 \cong q_2^2 \cong 0$
- small ball translational velocity: $\dot{q}_1^2 \cong \dot{q}_2^2 \cong 0$.

Applying the proposed assumptions, the effects of the Coriolis and centrifugal forces can be neglected from the equations of motion, yielding a dynamical model as:

$$\begin{aligned}
&\left(m_b + \frac{J_b}{r^2} \right) \ddot{q}_1 - m_b r \ddot{q}_3 + \mathrm{g} m_b q_3 = 0, \\
&\left(m_b + \frac{J_b}{r^2} \right) \ddot{q}_2 - m_b r \ddot{q}_4 + \mathrm{g} m_b q_4 = 0, \\
&\left(m_p \frac{w^2}{12} + m_b r^2 \right) \ddot{q}_3 - m_b r \ddot{q}_4 + m_b \mathrm{g}(q_1 - r q_3) = T_1, \\
&\left(m_p \frac{w^2}{12} + m_b r^2 \right) \ddot{q}_4 - m_b r \ddot{q}_2 + m_b \mathrm{g}(q_2 - r q_4) = T_2.
\end{aligned} \tag{21}$$

By comparing the masses of the ball and the plate, it can be concluded that the ball mass is much smaller than the plate mass. If $m_b << m_p$, then the influence of the ball dynamics on the plate dynamics in Eq. (21) can be neglected. Using Eq. (18) and Eq. (20), the simplified linearized mathematical model is given as:

$$\begin{aligned}
\ddot{q}_1 &= -\frac{5}{7} \mathrm{g} p_3 + \frac{60 r K_1}{7 m_p w^2} \Delta p_1, \\
\ddot{q}_2 &= -\frac{5}{7} \mathrm{g} p_4 + \frac{60 r K_2}{7 m_p l^2} \Delta p_2, \\
\ddot{q}_3 &= \frac{12 K_1}{m_p w^2} \Delta p_1, \\
\ddot{q}_4 &= \frac{12 K_2}{m_p l^2} \Delta p_2, \\
\Delta \dot{p}_1 &= -\frac{1}{\tau_v} \Delta p_1 + \frac{K_v}{\tau_v} u_1, \\
\Delta \dot{p}_2 &= -\frac{1}{\tau_v} \Delta p_2 + \frac{K_v}{\tau_v} u_2.
\end{aligned} \tag{22}$$

From Eq. (22) the linearized state-space model is derived as:

$$\begin{aligned}
\boldsymbol{x} &= \boldsymbol{A}\boldsymbol{x} + \boldsymbol{B}\boldsymbol{u}, \\
\boldsymbol{y} &= \boldsymbol{C}\boldsymbol{x} + \boldsymbol{D}\boldsymbol{u},
\end{aligned} \tag{23}$$

where the state space variables are defined as

$$\boldsymbol{x} = \left[q_1, \dot{q}_1, q_2, \dot{q}_2, q_3, \dot{q}_3, q_4, \dot{q}_4, \Delta p_1, \Delta p_2 \right]^{\mathrm{T}}.$$

3.2 Controller Design

In this paper, the Linear Quadratic Regulator (LQR) will be used to stabilize a highly nonlinear system. The proposed controller will be designed to stabilize the system at the equilibrium point and will also be tested for tracking a circular trajectory. The LQR method is a state-feedback controller that determines the optimal gains for the state variables based on two matrices, $\boldsymbol{Q}$ and $\boldsymbol{R}$. The matrices $\boldsymbol{Q}$ and $\boldsymbol{R}$ are selected iteratively, with a good starting point for the parameters chosen as:

$$\begin{aligned}
Q_{ii} &= \frac{1}{\max(x_i)^2}, \\
r &= \frac{1}{\max(u)^2},
\end{aligned} \tag{24}$$

where x_i is the maximum deviation of the state-space variable and u is the maximal controller output.

The infinite-horizon, continuous-time LQR controller is based on minimizing the following performance criterion:

$$J = \int_0^\infty (\boldsymbol{x}^{\mathrm{T}} \boldsymbol{Q} \boldsymbol{x} + \boldsymbol{u}^{\mathrm{T}} \boldsymbol{R} \boldsymbol{u}) \mathrm{d}t, \tag{25}$$

where the feedback control law that minimizes the value of the cost is $\boldsymbol{u} = \boldsymbol{K}\boldsymbol{x}$.

4 SIMULATION AND EXPERIMENTAL RESULTS

Numerical simulations are based on the state-space model from Eq. (23) and the LQR controller. The parameters used for the numerical simulation are shown in Tab. 1. Simulations are performed in Matlab using the ODE routine.

Table 1 Parameters of the ball and plate system

Symbol	Parameter	Value
m_b	mass of the ball	0.067 kg
m_p	mass of the plate	2.7 kg
r	radius of the ball	0.013 m
w	width of the plate	0.360 m
l	length of the plate	0.290 m
g	acceleration due to gravity	9.81 m/s2
D_0	nominal diameter of the muscle	0.01 m
α_0	initial angle of the braided shell	22 deg
ϵ_0	initial contraction ratio of the muscle	0.1
K_v	gain of the proportional valve	1.1105 Pa/V
τ_v	time constant of the proportional valve	0.05 s

Fig. 4 shows the simulation results for the simplified and linearized dynamical model from Eq. (23). The results demonstrate good performance in stabilizing the ball at the equilibrium point, as well as a strong response to external disturbances.

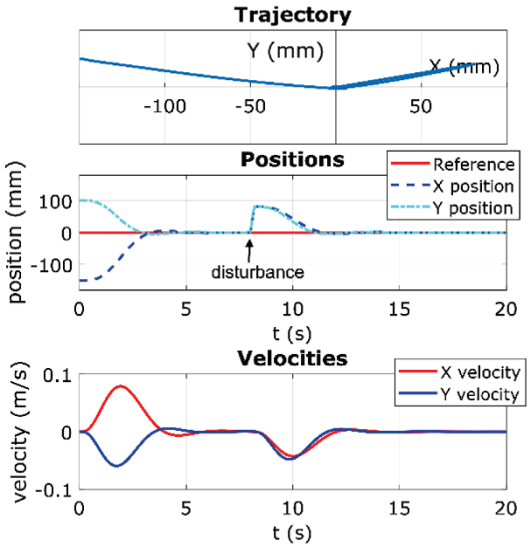

Figure 4 Simulation results - equilibrium point with disturbances

Experimental results for stabilizing the ball at the equilibrium point and for tracking the desired trajectory are shown in Fig. 5 and Fig. 6. The first diagram shows the ball trajectory in the *XY* plane. The second diagram displays the *X*, *Y*, and reference ball positions, while the third diagram presents the ball velocities. In both cases, the LQR controller demonstrated strong performance. High-amplitude external disturbances, during the ball stabilization at the equilibrium point, were effectively rejected by the LQR controller within approximately 5 seconds, with minimal deviation from the center of the plate. The experimental results also show that the LQR controller can track the circular trajectory of the highly nonlinear system actuated by pneumatic muscles, with only a small deviation from the reference trajectory.

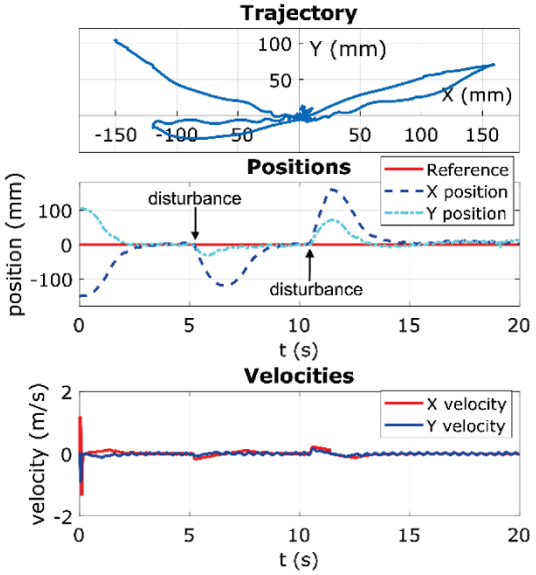

Figure 5 Experimental results - equilibrium point with disturbances

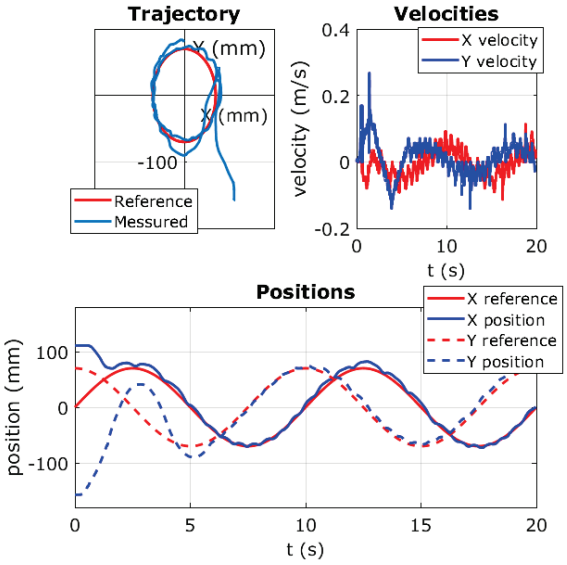

Figure 6 Experimental results - trajectory tracking

5 CONCLUSION

In this paper, a nonlinear mathematical model of the ball and plate mechanism actuated by pneumatic muscles is derived using the Lagrangian method. Nonlinearities due to air compressibility, pneumatic muscles, and the proportional valve were simplified and represented using a first-order lag term. The linearized model was derived around an equilibrium point with certain assumptions and approximations. The LQR controller was derived from the linearized model, and simulation results demonstrated good performance in stabilizing the ball at the equilibrium point and in trajectory tracking.

Experimental results showed minimal deviation from the simulation results for the LQR controller and confirmed that the simplifications and assumptions made during the linearization process had a minimal impact on the system dynamics. However, while LQR control proved effective, it

may not be optimal for handling large nonlinearities. More advanced adaptive control strategies, such as Model Predictive Control (MPC) or Reinforcement Learning (RL), could be explored in future work to improve performance.

Furthermore, while the study simplified the pneumatic artificial muscles (PAMs) using a first-order lag model, PAMs inherently exhibit additional nonlinearities such as hysteresis and air compressibility effects. A more detailed modeling approach could enhance accuracy and provide a deeper understanding of the system dynamics. Additionally, the experimental validation focused on short-term performance, whereas a long-term analysis, considering environmental variations such as temperature and air pressure fluctuations, could offer insights into the system's robustness.

The comparison between experiment and simulations was limited to a single parameter setting, which may not capture the full range of system behavior. A more comprehensive Design of Experiments (DoE) approach could help explore model sensitivities and improve generalizability.

6 REFERENCES

[1] Rose, C. G., Bucki, N. & O'Malley, M. K. (2017). A ball and beam module for a haptic paddle education platform. *American Society of Mechanical Engineers, 3*. https://doi.org/10.1115/DSCC2017-5027

[2] Galvan-Colmenares, S., Moreno-Armendariz, M. A., de Jesus Rubio, J., Ortíz-Rodriguez, F., Yu, W. & Aguilar-Ibanez, C. F. (2014). Dual PD control regulation with nonlinear compensation for a ball and plate system. *Mathematical Problems in Engineering, 2014*, 1-10. https://doi.org/10.1155/2014/894209

[3] Liu, H. & Liang, Y. (2010). Trajectory tracking sliding mode control of ball and plate system. In *The 2nd IEEE International Asia Conference on Informatics in Control, Automation and Robotics (CAR 2010)*, 1-5.

[4] Aphiratsakun, N. & Otaryan, N. (2016). Ball on the plate model based on PID tuning methods. In *The 13th International Conference on Electrical Engineering/Electronics, Computer, Telecommunications and Information Technology (ECTI-CON2016)*, 1-4. https://doi.org/10.1109/ECTICon.2016.7561324

[5] Dusek, F., Honc, D. & Sharma, K. R. (2017). Modelling of ball and plate system based on first principle model and optimal control. In *The 21st IEEE International Conference on Process Control (PC2017)*, 1-5. https://doi.org/10.1109/PC.2017.7976216

[6] Debono, D. & Bugeja, M. (2015). Application of sliding mode control to the ball and plate problem. In T*he 12th International Conference on Informatics in Control, Automation and Robotics (ICINCO2015), 01*, 412-419. https://doi.org/10.5220/0005569804120419

[7] Mani, G., Sivaraman, N. & Kannan, R. (2018). Visual servoing based model reference adaptive control with Lyapunov rule for a ball on plate balancing system. In *IEEE International Conference on Intelligent and Advanced System (ICIAS2018)*, 1-6. https://doi.org/10.1109/ICIAS.2018.8540635

[8] Fan, X., Zhang, N. & Teng, S. (2004). Trajectory planning and tracking of ball and plate system using hierarchical fuzzy control scheme. *Fuzzy Sets and Systems, 144*(2), 297-312. https://doi.org/10.1016/j.fss.2003.11.008

[9] Dong, X., Zhang, Z. & Chen, C. (2009). Applying genetic algorithm to on-line updated PID neural network controllers for ball and plate system. In *Fourth IEEE International Conference on Innovative Computing, Information and Control (ICICIC2009)*, 1-4. https://doi.org/10.1109/ICICIC.2009.113

[10] Mochizuki, S. & Ichihara, H. (2013). I-PD controller design based on generalized KYP lemma for ball and plate system. In *IEEE European Control Conference (ECC2013)*, 1-6. https://doi.org/10.23919/ECC.2013.6669269

[11] Azman, M. A., Faudzi, A. A. M., Mustafa, N. D., Osman, K. & Natarajan, E. (2014). Integrating servopneumatic actuator with ball beam system based on intelligent position control. *Jurnal Teknologi, 69*(3), 47-53. https://doi.org/10.11113/jt.v69.3146

[12] Šitum, Ž. & Trslić, P. (2018). Ball and beam balancing mechanism actuated with pneumatic artificial muscles. *Journal of Mechanisms and Robotics, 10*(5), 1-8. https://doi.org/10.1115/1.4040103

[13] Zhao, W. (2013). A study of the ball-and-plate system driven by pneumatic direct cylinders. *Applied Mechanics and Materials, 310*, 294-303. https://doi.org/10.4028/www.scientific.net/AMM.310.294

[14] Scaff, W., Horikawa, O. & de Sales Guerra Tsuzuki, M. (2018). Pneumatic artificial muscle optimal control with simulated annealing. *IFAC-PapersOnLine, 51*(27), 333-338. https://doi.org/10.1016/j.ifacol.2018.08.141

[15] Tondu, B. & Lopez, P. (2000). Modeling and control of McKibben artificial muscle robot actuators. *IEEE Control Systems Magazine, 20*(2), 15-38. https://doi.org/10.1109/37.846122

[16] Schroder, J., Erol, D., Kawamura, K. & Dillman, R. (2003). Dynamic pneumatic actuator model for a model-based torque controller. In *Proceedings IEEE International Symposium on Computational Intelligence in Robotics and Automation*, 1-6. https://doi.org/10.1109/CIRA.2003.1243644

Authors' contacts:

Juraj Benić, PhD, Assistant Professor
(Corresponding author)
School of Applied Mathematics and Computer Science, University of Osijek,
Trg Ljudevita Gaja 6, 31000 Osijek, Croatia
jbenic@mathos.hr

Andreas Šantek
University of Zagreb,
Faculty of Mechanical Engineering and Naval Architecture,
Ivana Lučića 5, 10000 Zagreb, Croatia
andreassantek@hotmail.com

Željko Šitum, PhD, Full Professor
University of Zagreb,
Faculty of Mechanical Engineering and Naval Architecture,
Ivana Lučića 5, 10000 Zagreb, Croatia
zeljko.situm@fsb.unizg.hr